Detailed study of non-stationary elastic wavefields produced by an apodized normal transducer. Comparisons between asymptotics and numerical results

E. Bécache[†,*], **A. Kiselev**[‡,*]
Projet Ondes, [†]INRIA Rocquencourt, UMR 27-06 CNRS-INRIA-ENSTA, France
[‡]Steklov Mathematical Institute, St.Petersburg Department, Fontanka 27, St.Petersburg, Russia
[*]Email: eliane.becache@inria.fr, kiselev@pdmi.ras.ru

Introduction

We simulate non-stationary near-field of a phased transducer at the surface of an isotropic homogeneous elastic half-space. The transducer is assumed large compared to the characteristic wavelength.

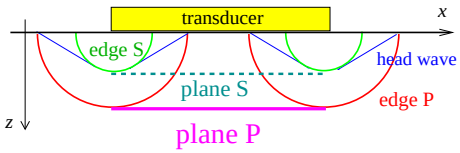

Figure 1: Wavefronts

We focus on effects of non-uniformity of pressure (see Fig. 2). Predictions of the asymptotic theory [1],

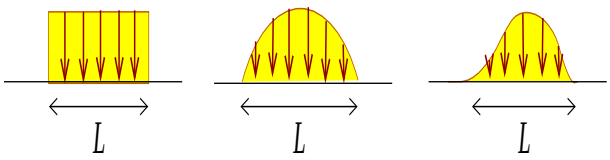

Figure 2: Pressure distribution on the transducer aperture

[2], [3], [4], [5] are tested against numerics and their agreement is found excellent.

Mathematical formulation

The 2D displacement field $\mathbf{u} = \mathbf{u}(x,z,t)$ is described by

$$\frac{1}{V_p^2}\text{grad div}\mathbf{u} - \frac{1}{V_s^2}\text{rot rot}\mathbf{u} - \frac{\partial^2 \mathbf{u}}{\partial t^2} = 0,\ z > 0, \tag{1}$$

V_p and V_s are velocities of P- and S-waves, and the boundary stresses are

$$\sigma_{xx}|_{z=0} = \sigma_{xz}|_{z=0} = 0,\ \ \sigma_{zz}|_{z=0} = P(x)F(t). \tag{2}$$

Here σ_{xx} and σ_{xz} are tangent components of the linear stress tensor, and σ_{zz} its normal component, $P(x)$ is the density of the external pressure distribution on the boundary, and $F(t)$ is the input signal. We also assume the initial conditions

$$\mathbf{u}|_{t=0} = 0,\ \ \partial\mathbf{u}/\partial t|_{t=0} = 0.$$

We apply the numerical method [6], [7] based on a velocity-stress formulation, where the velocity field is

$$\mathbf{v} = \partial\mathbf{u}/\partial t,$$

and for convenient reasons we will work with the velocity in the following.

Asymptotic theory

Let F_c be the characteristic frequency of the signal $F(t)$, $k_p = 2\pi F_c/V_p$ characteristic P-wavenumber, L the size of the transducer.

We assume that the transducer is large,

$$k_p L >> 1, \tag{3}$$

that the pressure density $P(x)$ is smooth on the transducer aperture and that the near-zone condition holds

$$k_p L^2/z >> 1, \tag{4}$$

where z is the depth of observation points.

0.1 'Main' components of plane waves

For the 'main' components of P- and S-waves the asymptotic theory [4], [8], [5] predicts:

$$\begin{aligned} v_z^P(x,z,t) &= \frac{P(x)}{\rho V_p} F(t - z/V_p), \\ v_x^S(x,z,t) &= \frac{2V_s}{\rho V_p} P'(x) \int_{-\infty}^{t-z/V_s} F(s)ds, \end{aligned} \tag{5}$$

ρ being the volume density. The first formula is obvious while the second is sophisticated. No plane S-wave exist for the constant pressure density.

0.2 Anomalous, or additional components of plane waves

In reality, P-wave has also a transverse component and the S wave a longitudinal component (e. g.[1], [2]). For the above plane waves we have, respectively, the following expressions for the 'additional' components

$$\begin{aligned} v_x^P(x,z,t) &= -V_p \int_{-\infty}^{t-z/V_p} \frac{\partial}{\partial x} v_z^P(x,z,\tau)d\tau, \\ v_z^S &= V_s \int_{-\infty}^{t-z/V_s} \frac{\partial}{\partial x} v_x^S(x,z,\tau)d\tau. \end{aligned} \tag{6}$$

Formulas (5),(6) will be checked in the course of simulations of total wavefield.

The numerical method

We use a numerical method developed in [6] for solving propagation and diffraction problems in heterogeneous anisotropic media. This method is based on the velocity-stress formulation.

In [6], [7], new mixed finite elements, the so-called $Q_1^{\rm div} - Q_0$ element, based on the use of a regular grid in space have been introduced in order to approximate this formulation. Their main specificity is that they lead to an explicit scheme in time, thanks to the fact that all the degrees of freedom of the stress tensor are located at the same nodes. We only summarize here the properties of the scheme: second order and explicit in time, second order and based on a regular quadrilateral mesh in space (implementation like finite differences), taking into account the symmetry of the stress tensor in a strong way. We refer to [6], [7] for more details on these elements (convergence analysis, dispersion analysis...).

Numerical simulations

In this section, we consider a domain $0 < x < L_x$, $0 < z < L_z$, with $L_x = 20$, $L_z = 10$ (see Fig 3). The time domain signal is defined as

$$F(t) = \begin{cases} \sin(2\pi F_c t), & \text{in } [0, \frac{1}{2F_c}] \cup [\frac{1}{F_c}, \frac{3}{2F_c}] \\ 2\sin(2\pi F_c t), & \text{in } [\frac{1}{2F_c}, \frac{3}{2F_c}] \\ 0, & \text{elsewhere} \end{cases} \qquad (7)$$

with $F_c = 1.9$. The velocities in the medium are $V_p = 2.78$ and $V_s = 1.42$, which gives a characteristic wave length for P waves of $\lambda_p = 1.46$.

The solution will be presented either on snapshots (at a fixed time), or at some fixed observation points (with respect to time), located at the same depth $z_{obs} = L_z/4$ (see Figure 3).

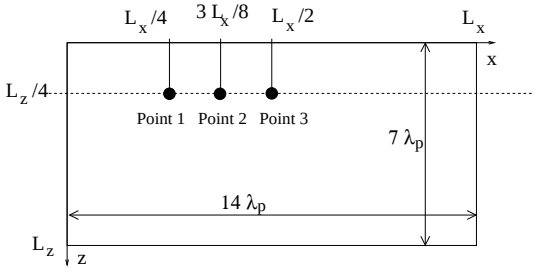

Figure 3: The computational domain and the observation points

Role of the smoothness of the pressure field

In this numerical experiment, we investigate the role of the smoothness of the pressure field on the strength of edge waves. We consider here a pressure imposed on a large transducer, of length equal to $L = 16 >> \lambda_p = 1.4$, so that both assumptions (4) and (3) are satisfied. The simulations are done with three different pressure fields: (1) discontinuous, (2) continuous (C^0), (3) differentiable (C^1). When the pressure is constant for $-\infty < x < +\infty$, we would have only a downgoing P-wave. Edge and head waves are predicted (by asymptotic theory not discussed here (see e.g. [3]) from the points where $P(x)$ is not smooth.

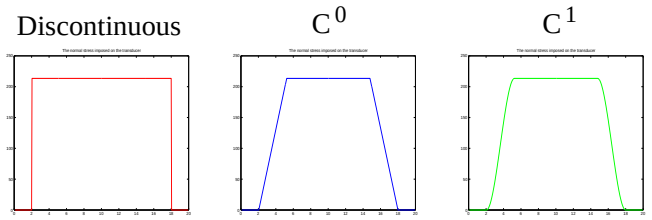

Figure 4: Normal stresses imposed at the surface

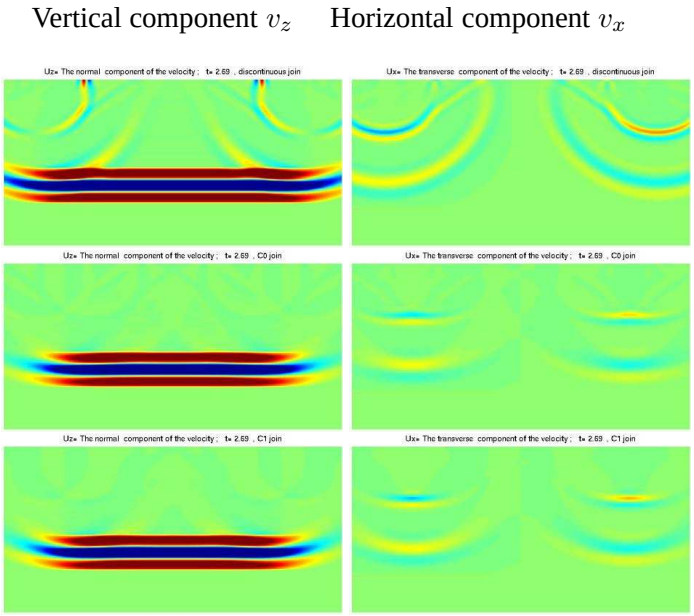

Figure 5: Influence of the smoothness of the pressure field. Top: discontinuous pressure. Middle: C^0 pressure. Bottom: C^1 pressure.

In Figure 5 we represent the two components of the computed field, for the three pressure fields (with the same scale), at time $t = 2.7s$. The vertical component v_z is mainly composed with the plane P-wave. For a discontinuous pressure we observe strong P and S edge waves and some head waves. Their amplitudes strongly decrease in the C^0 case and no significant difference is seen with the C^1 one. The horizontal component v_x of the plane P-wave should be zero where $P(x)$ is constant and really the field is mainly composed of P and S edge waves whose amplitudes decrease with the C^0 pressure field.

We now observe in Figure 6 the comparison between the computed vertical component v_z along the time and the asymptotically predicted component for a constant pressure v_z^P, at the two observation points: point 1 and

point 3 (see Fig. 3). We observe a good agreement between asymptotics and numerics. It is particularly good for C^0 and C^1 pressures. Minor differences for the case of discontinuous pressure are due to the presence of strong edge waves, for which we did not apply here any asymptotics.

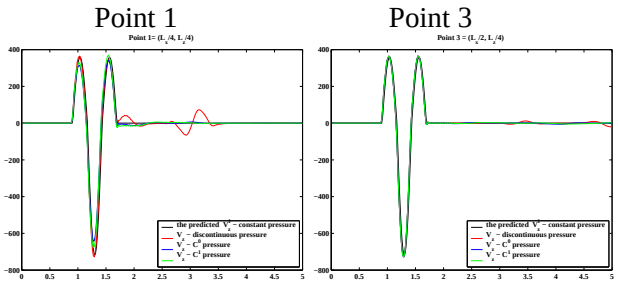

Figure 6: Comparison between the predicted v_z^P for a constant pressure field and the computed v_z for a (1) discontinuous, (2) C^0, (3) C^1 pressure field

Role of the size of the transducer for a regular pressure field

We now compare the asymptotic and numerical fields for a regular pressure field whose aperture varies from $L = L_x$ to $L = 0.1L_x$ (see Figure 7). In terms of the P wavelength, the four transducer's length are $L = 13\lambda_p$, $L = 8\lambda_p$, $L = 5\lambda_p$, $L = 1.3\lambda_p$.

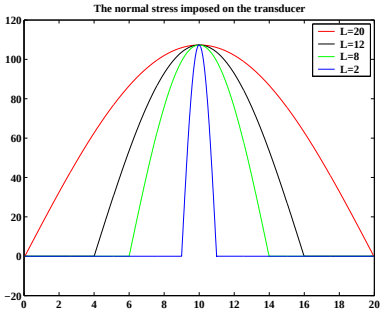

Figure 7: Normal stresses imposed at the surface

Snapshots, represented in Fig. 8, show that for the three largest transducers, i.e. until $L \geq 5\lambda_p$, the vertical component of the velocity v_z is mainly composed of a plane P-wave, as predicted by the asympotics. However, some (rather small) edge waves appear when the size decreases. Concerning the horizontal component v_x, it is not only composed with a plane S-wave, but also with a strong additional component of the plane P-wave (6). For the last transducer, whose length is of the same order as the P wavelength, it clearly acts as a point source and does not produce plane waves, since the assumption (3) is not satisfied anymore.

We now compare in Figure 9 the asymptotic predictions with the computed field, at the observation Point 2

Vertical component v_z Horizontal component v_x

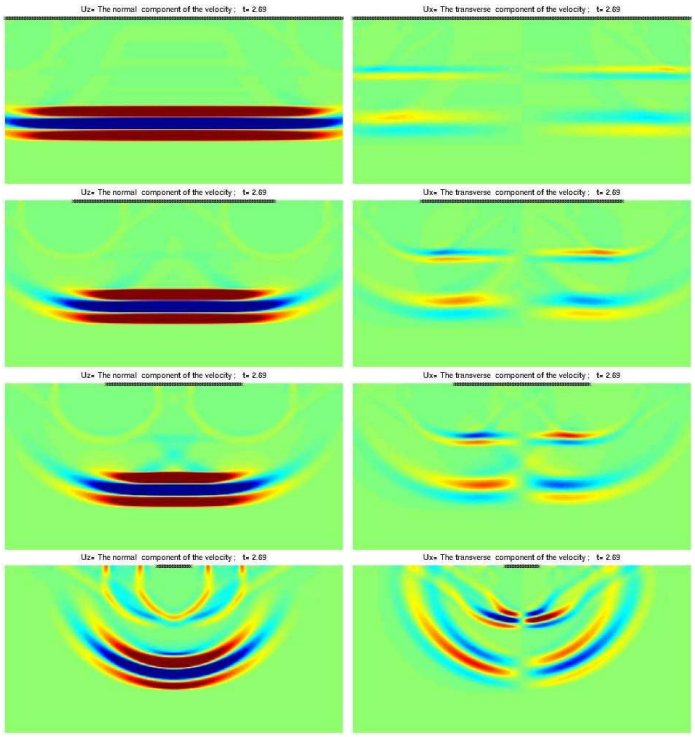

Figure 8: Snapshots at $t = 2.7s$. From top to bottom: $L = 20$, $L = 12$, $L = 8$, $L = 2$

(see Fig. 3). The left column corresponds to the results for the vertical component and the right one to the horizontal component. On each figure, we have represented the computed field, the predictions with the "main" and additional components. Concerning the vertical component v_z, the asymptotic predictions v_z^P and $v_z^P + v_z^S$ coincide very well with the computed field, for the three transducers satisfying $L \geq 5\lambda_p$. Actually the additional component v_z^S is negligible. On the other hand, concerning the horizontal component, one clearly observes the first arrival, corresponding to the additional component of plane P wave, which is approximately of the same amplitude as the "main" component of the plane S-wave v_x^S. Taking into account the additional component (6) of the P wave was necessary to have a good agreement for the largest transducer. Small differences between asymptotics and numerics appear for $L = 8\lambda_p$, becoming larger for $L = 5\lambda_p$ but still not too large. Finally, according to the comments on the snapshots, asymptotics and numerics become very different for the smallest transducer $L = 1.3\lambda_p$, in which case the observation point is not anymore under the transducer, and assumption (3) is clearly not satisfied.

Conclusion

In conclusion, the asymptotic theory predicts the solution in a very accurate way, provided that : (i) the

v_z, v_z^P and $v_z^P + v_z^S$ $\qquad$ v_x, v_x^S and $v_x^S + v_x^P$

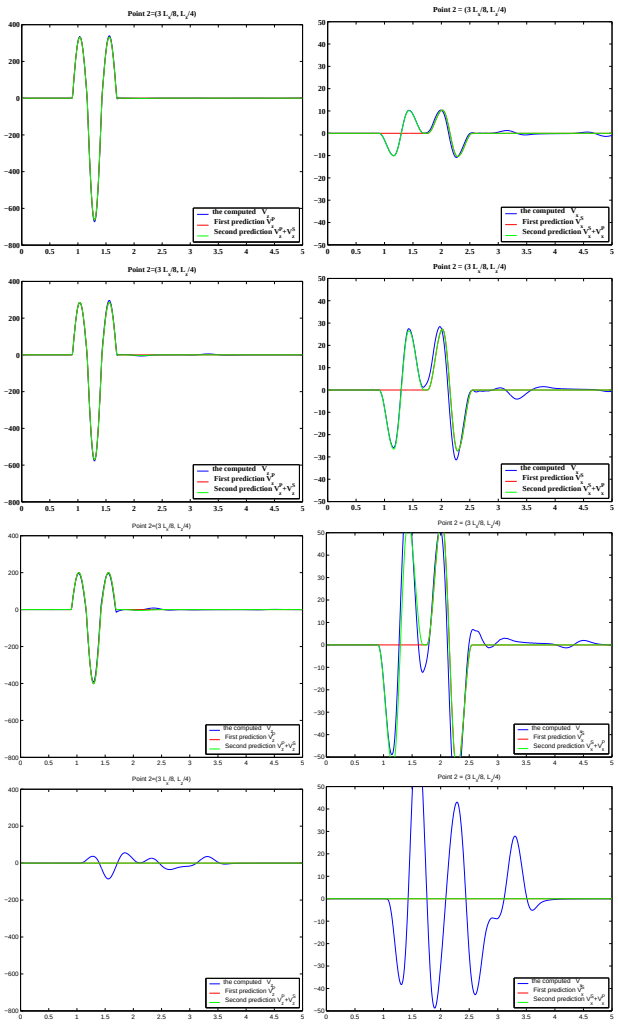

Figure 9: Comparison between the asymptotic predictions and the numerical solution, at observation Point 2, for a regular pressure field. From top to bottom: (1) $L = 20$, (2) $L = 12$, (3) $L = 8$, (4) $L = 2$

pressure field is smooth enough, so that it does not produce too strong edge waves, (ii) the transducer is "large" enough compared to the P-wavelength (at least five times the wavelength).

Also, such predictions of the asymptotic theory as: (i) the existence of the plane S-wave for a non-constant pressure, (ii) the suppression of edge waves by taking smooth transducers, are confirmed by numerics.

Acknowledgments

Part of this work was carried out when the second author was invited at INRIA. This work was also supported by RFBR grant 020100260.

References

[1] A. P. Kiselev. Extrinsic component of elastic waves. *Phys. Solid Earth*, 19(9):707–710, 1983.

[2] L. Ju. Fradkin and A. P. Kiselev. The two-component representations of time-harmonic elastic body waves at high- and intermediate-frequency regimes. *JASA*, 101(1):52–65, 1997.

[3] L. Ju. Fradkin, A. P. Kiselev, and E. Krylova. The radiating near-field asymptotics of a normal circular ultrasonic transducer in an elastic half-space. *JASA*, 104(3):1178–1186, 1998.

[4] A. P. Kiselev, E. Krylova, and L. Ju. Fradkin. Excitation of a quasi-plane shear wave by a surface acoustic source producing normal stresses. *Tech. Phys. Lett.*, 23(23):941–942, 1997.

[5] A. P. Kiselev and A. A. Klimova. A plane shear wave excited in an elastic half-space by oscillating normal pressure distributed nonuniformly. *J. Math. Sci.*, 108(5):703–709, 2002.

[6] E. Bécache, P. Joly, and C. Tsogka. Fictitious domains, mixed finite elements and perfectly matched layers for 2d elastic wave propagation. *J. Comp. Acous.*, 9(3):1175–1203, 2001.

[7] E. Bécache, P. Joly, and C. Tsogka. A new family of mixed finite elements for the linear elastodynamic problem. *SIAM J. Numer. Anal.*, 39(6):2109–2132 (electronic), 2002.

[8] D. Gridin. On radiation of ultrasound into an isotropic elastic half-space via wavefront expansions of the impulse response. *JASA*, 105(5):2565–2573, 1999.